



## Original article

# Consolidated effect of fiber-reinforcement and concrete strength class on mechanical performance, economy and footprint of concrete for pavement use

Babar Ali <sup>a,\*</sup>, Erol Yilmaz <sup>b</sup>, Muhammad Sohail Jameel <sup>c</sup>, Waqas Haroon <sup>d</sup>, Rayed Alyousef <sup>e</sup>

<sup>a</sup> Department of Civil Engineering, COMSATS University Islamabad, Sahiwal Campus, Sahiwal 57000, Pakistan

<sup>b</sup> Department of Civil Engineering, Geotechnical Division, Recep Tayyip Erdogan University, Fener, Rize TR53100, Turkey

<sup>c</sup> Department of Transportation Engineering and Management, University of Engineering and Technology, G.T. Road, Lahore 54890, Pakistan

<sup>d</sup> Department of Civil Engineering, International Islamic University, Islamabad 47050, Pakistan

<sup>e</sup> Department of Civil Engineering, College of Engineering, Prince Sattam bin Abdulaziz University, Alkharij 16273, Saudi Arabia

## ARTICLE INFO

## Article history:

Received 28 January 2021

Accepted 27 September 2021

Available online xxx

## Keywords:

Compressive and flexural strength

Flexural toughness

Fibers

Environment

Concrete road

## ABSTRACT

The advancement in the tensile strength and ductility of plain concrete can minimize the quantity of materials required per unit strength to build eco-friendly structures. This paper compares the compressive and flexural behavior of different strength classes (C20, C30, and C45) of concrete with the varying volume fractions of hooked steel fiber (HSF) considering the application of concrete road. The performance of each strength class was evaluated and compared based on the compressive and tensile testing results. Using the mechanical properties of concrete mixtures; the design thickness, cost, and global warming potential of concrete pavement were calculated and compared between different mixes under the same traffic loadings. The results showed that the maximum utilization of HSF was observed in the high-strength C45, whereas HSF showed comparatively low efficiency in low-strength C20. At 0.25% volume of HSF, low strength C20 concrete showed higher residual strength and flexural toughness than that of the plain high strength C45 concrete. The analysis of design thickness of pavements revealed that low-strength C20 at 0.25–0.5% HSF can provide cost-effective and eco-friendly pavements compared to a plain high strength C45 for the same design loadings. The results of this study provide useful insights on the selection of strength class and concentration of steel fiber for pavement application.

© 2021 The Authors. Production and hosting by Elsevier B.V. on behalf of King Saud University. This is an open access article under the CC BY license (<http://creativecommons.org/licenses/by/4.0/>).

**Abbreviations:**  $E_C$ , Modulus of elasticity;  $f_R$ , Flexural strength;  $f_{RS}$ , Residual flexural strength;  $f_{CS}$ , Compressive strength;  $GWP$ , Global warming potential; HSF, Hooked steel fiber;  $h_{Design}$ , Design thickness of pavement; JPCP, Jointed-plain concrete pavement;  $T_R$ , Flexural toughness.

\* Corresponding author.

E-mail addresses: [babar.ali@sctwuh.edu.pk](mailto:babar.ali@sctwuh.edu.pk), [babar.ali@cuisahiwal.edu.pk](mailto:babar.ali@cuisahiwal.edu.pk) (B. Ali), [erol.yilmaz@erdogan.edu.tr](mailto:erol.yilmaz@erdogan.edu.tr) (E. Yilmaz), [Sohail.jameel@uet.edu.pk](mailto:Sohail.jameel@uet.edu.pk) (M. Sohail Jameel), [waqas.haroon@iiu.edu.pk](mailto:waqas.haroon@iiu.edu.pk) (W. Haroon), [r.alyousef@psau.edu.sa](mailto:r.alyousef@psau.edu.sa) (R. Alyousef).

Peer review under responsibility of King Saud University.



Production and hosting by Elsevier

<https://doi.org/10.1016/j.jksues.2021.09.005>

1018-3639/© 2021 The Authors. Production and hosting by Elsevier B.V. on behalf of King Saud University.

This is an open access article under the CC BY license (<http://creativecommons.org/licenses/by/4.0/>).

Please cite this article as: B. Ali, E. Yilmaz, M. Sohail Jameel et al., Consolidated effect of fiber-reinforcement and concrete strength class on mechanical performance, economy and footprint of concrete for pavement use, Journal of King Saud University – Engineering Sciences, <https://doi.org/10.1016/j.jksues.2021.09.005>

presents many benefits i.e., good distribution of reinforcement throughout the concrete matrix, reduction in the tensile cracking, increase in compressive toughness,  $T_R$ , and  $f_{RS}$  (Afrouhsabet et al., 2017; Balendran et al., 2002; Carneiro et al., 2014; Fareed et al., 2021).

An integration of fiber-reinforcement gives rise to a drop in the quantity of material (i.e., cement and aggregates) required per unit strength. Therefore, the utilization of fibers in concrete also offers sustainability benefits by reducing the demand for raw materials of concrete. Ahmadi et al. (2017) showed that incorporating 1% recycled steel fibers into concrete leads to a decrease of 70 mm in the pavement design thickness. Chan et al. (2019) have also mentioned the environmental benefits of using fiber-reinforced recycled aggregate concrete in pavements. The main reason for the reduction in pavement thickness is the improvement in  $f_R$  and  $f_{RS}$  of concrete with the addition of fiber (Ali et al., 2020a; Raza et al., 2020b).

Various types of fibers (i.e., steel, polypropylene, glass, carbon, and basalt fiber) are currently being used in the construction industry, and their effects have been evaluated experimentally on concrete's strength and stability properties. Fiber addition does not only enhances strength properties, but it also shows positive effects on the resistance of concrete against freeze–thaw and drying shrinkage (Karahana and Atiş, 2011; Zhang and Li, 2013). The main reason for the improvement in the durability as a result of fiber-reinforcement can be well explained by the increase in the binder's tensile capacity that prevents the volumetric changes causing the damage in plain concrete under the actions of freeze–thaw cycles and dry shrinkage. Fibers also improve the fire-resistance of concrete (Al Qadi and Al-Zaidyeen, 2014).

Steel fibers have shown better performance compared to other fibers (e.g., carbon, glass, polypropylene, etc.) in terms of efficiency in enhancing the mechanical performance of plain concrete (Afrouhsabet et al., 2018; Afroz et al., 2019; Algburi et al., 2019; Raza et al., 2020b). It also shows better bonding with the binder matrix when compared to polypropylene, carbon, and glass fibers (Ali et al., 2020b; Raza et al., 2020a). A strong bond with the binder matrix ensures the maximum efficacy of fiber-reinforcement in enhancing the concrete's strength capacity. Furthermore, the use of hooked steel fiber (HSF) significantly enhances the bond-strength of fibers incorporating binder. According to Afrouhsabet et al. (2017), the HSF usage of 1% can augment the  $f_{CS}$ ,  $f_{SP}$ , and  $f_R$  of concrete by 10%, 45%, and 80%, respectively. These improvements in mechanical performance due to HSF addition are phenomenal compared to those caused by the use of plain steel fiber that enhances the  $f_{CS}$ ,  $f_{STS}$ , and  $f_R$  of concrete by 7%, 24%, 25%, respectively (Ali et al., 2020b).

A large number of studies can be found in the existing literature reporting the benefits of fiber-reinforced concrete in terms of advancing mechanical and durability performance. However, very limited information is available on the performance evaluation of different strength classes of concrete with the varying percentages of HSF. Besides that very few studies (Ahmadi et al., 2017; Chan et al., 2019) analyzed the performance of fiber-reinforced mixes considering their application in pavement structures and no data is available on the economic and carbon footprint analysis of the application of HSF-reinforced concrete. Generally, fibers are costlier than conventional raw materials of concrete. Not only the cost of fiber-reinforcement is a major concern to the economy of concrete production, but also the increment in the demand for the superplasticizer to compensate for the loss of workability, significantly increases the final cost of concrete. On the other hand, the accomplished benefits, such as improved  $f_R$ ,  $f_{STS}$ , and  $f_{RS}$  due to fiber addition should also be regarded while assessing the economy of fiber-reinforced concretes.

The primary objective of the present work is to evaluate the compressive and flexural behavior of different strength classes of laboratory-prepared concrete mixtures with varying HSF volume fractions. The mechanical performance of mixtures was assessed by the following parameters, such as compressive strength-  $f_{CS}$ , modulus of elasticity- $E_C$ , flexural strength- $f_R$ , flexural toughness- $T_R$ , and residual flexural strength- $f_{RS}$ . The secondary objective of this work is to analyze the  $h_{Design}$ , cost, and GWP of JPCP using the mechanical properties of the studied mixtures under the same conditions of traffic loadings and design life.

## 2. Materials and methods

### 2.1. Material characterization

In this study, Type I Portland cement (53 Grade) qualifying to ASTM-C150 (2018) was utilized as a binder. Fine aggregate was the siliceous sand of Lawrancepur quarry having a fineness modulus of 2.54. Crushed limestone as coarse aggregate was obtained from one of the quarries of Margalla hills, Taxila, Islamabad. The highest particle size of coarse and fine aggregates was 25 mm and 4.75 mm, respectively. The key properties of both fine and coarse aggregate are given in Table 1. The gradation of both of these aggregates is within the limits recommended by ASTM C33 (2018) for concrete aggregates. HSF (Fig. 1) has the key properties given in Table 2. These fibers were glued with a water-soluble chemical (anti-corrosion) and these were easily dismantled during the blending process. The diameter and length of HSF were 0.9 and 35 mm, respectively and these dimensions were chosen because of the local availability, while, longer fibers can also be used for more effectiveness (Han et al., 2019). Viscocrete 3110 was the superplasticizer used to attain the target slump of 50 mm in the case of HSF-reinforced mixes.

### 2.2. Design of concrete mixes

In this study, a total of 12 concrete mixtures were produced, details are provided in Table 3. Three different strength classes of concrete were produced (low-strength-C20, normal-strength-C30, and high-strength-C45). In each of these three strength classes of concrete, four different volume fractions of HSF were used as 0%, 0.25%, 0.5%, and 1%, respectively. ACI-211 (2000) was used for the design of strength classes of concrete i.e. C20 ( $f_{CS} = 20$  MPa), C30 ( $f_{CS} = 30$  MPa) and C45 ( $f_{CS} = 45$  MPa). The slump value for all strength classes was selected as 50 mm which is considered a typical slump used for pavement concrete. In the case of fiber-reinforced mixtures, to compensate for the loss in workability, superplasticizer (SP) was used as 0.25%, 0.35%, and 0.65% by mass of cement for 0.25%, 0.5% and 1% dose of steel fiber, respectively. The entire constituents of concretes were blended in a mixer with adjustable rotational speed. Firstly, all aggregates and binders were dry blended for 2 mins at a speed of 40 rpm. In the second stage, half of the amount of water and plasticizer was added, and the blending process continued for 2 mins at 60 rpm. In the third stage,

**Table 1**  
Key properties of the aggregates used in the experiments.

Property	Fine aggregate	Coarse aggregate
Material	Siliceous sand	Crushed limestone
Water absorption (%)	1.12	0.78
Maximum size of particles (mm)	4.75	25
Fineness modulus	2.54	–
Specific gravity	2.65	2.68
Dry rodded density ( $\text{kg/m}^3$ )	1620	1550

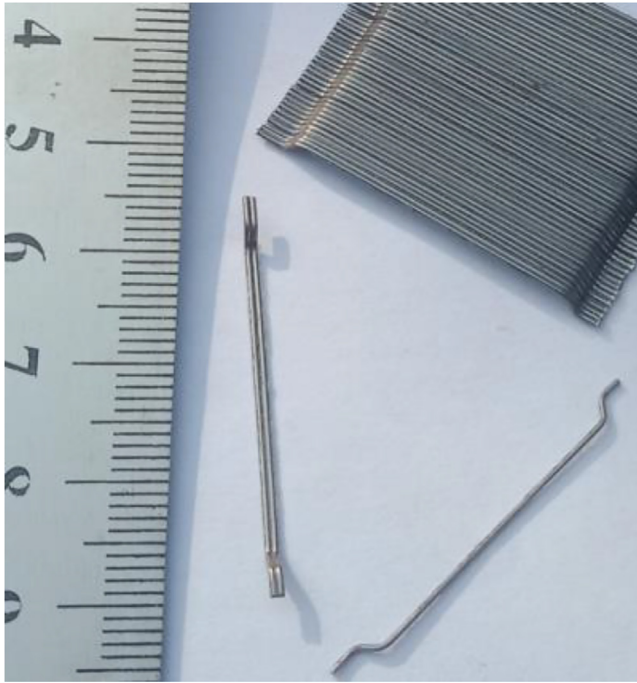


Fig. 1. Hooked steel fiber (HSF).

Table 2  
Properties of hooked steel fibers.

Property	Value
Length (mm)	35
Diameter ( $\mu\text{m}$ )	900
Tensile strength (MPa)	1200
Elastic modulus (GPa)	200
Density ( $\text{kg}/\text{m}^3$ )	7750

the remaining half amount of water and plasticizer was added and mixing continued for 2 mins at 60 rpm. Finally, HSF at the required percentage was added in the case of fiber-reinforced mixes, and the blending continued at a rapid speed of 80 rpm for 4 mins. The total duration of mixing lasted for 10 mins for both plain and HSF mixes. After mixing, the slump consistency was measured to check the workability of the mixes. If the average value of three slumps for each mix was within 45–55 mm, the casting stage proceeded, otherwise, the mix would be rejected, and new material was mixed again.

Table 3  
Engineering design of all concrete mixtures.

Mix ID	Cement (kg)	Water (kg)	Coarse aggregate (kg)	Fine aggregate (kg)	HSF (kg)	SP (%)	SP (kg)
C20-0%HSF	255	180	1075	865	0	0	0.00
C20-0.25%HSF	255	180	1072	862	19.5	0.24	0.61
C20-0.5%HSF	255	180	1069	859	39	0.35	0.89
C20-1%HSF	255	180	1062	852	78	0.64	1.63
C30-0%HSF	330	180	1075	796	0	0	0.00
C30-0.25%HSF	330	180	1072	793	19.5	0.24	0.79
C30-0.5%HSF	330	180	1069	790	39	0.35	1.16
C30-1%HSF	330	180	1062	783	78	0.64	2.11
C45-0%HSF	475	180	1075	650	0	0	0.00
C45-0.25%HSF	475	180	1072	647	19.5	0.24	1.14
C45-0.5%HSF	475	180	1069	643	39	0.35	1.66
C45-1%HSF	475	180	1062	637	78	0.64	3.04

\*SP: superplasticizer.

### 2.3. Mechanical testing of concrete mixes

The compressive behavior of concrete mixes was evaluated by conducting  $f_{CS}$  and  $E_C$  tests following ASTM C39 (2012) and ASTM C469 (2014), respectively. Cylindrical specimens ( $D \times H$ :  $100 \times 200$  mm) were used for both experiments. To evaluate the flexural behavior ( $f_{RS}$ ,  $f_R$ , and  $T_R$ ) of each mix,  $100 \times 100 \times 350$  mm specimens of all mixes were tested following ASTM C1609, 2019.  $f_R$  was calculated as per ASTM-C78 (2018a). The overview of flexural testing and a typical load-midspan deflection graph is shown in Fig. 2. Mechanical testing was conducted on 28-day cured specimens in normal water.

### 2.4. Parameters for the thickness design ( $h_{Design}$ ) of pavements

The  $h_{Design}$  of pavements for two different streets namely collector and major arterial were designed using the mechanical properties of mixes (e.g.,  $E_C$ ,  $f_R$  and  $f_{RS}$ ) following Portland cement association design guidelines and using StreetPave tool developed by American Concrete Pavement Association (ACPA) (Robert and Packard, 2007). For both streets, a JPCP was selected for  $h_{Design}$ . Details about the traffic spectrums and truck traffic over the design life of street pavements are shown in Table 4. Other global inputs and concrete material properties that were considered in the  $h_{Design}$  are given in Table 5. In the pavement design, the serviceability is a unitless number ranging from 0 (awful) to 5 (perfect) (Robert and Packard, 2007). Serviceability at the end of design life is never taken as 0 instead serviceability index of 2 (fair) is taken. A conservative reliability value is taken as 85% (AASHTO, 2009). Reliability is a concept of accounting for uncertainties in the design of pavements. The level of reliability varies depending upon the loading conditions or type of highway in rural or urban conditions. For the real mechanistic-based design of rigid pavement, cracking at the end of design life is assumed to be 15% due to variation in conditions and quality of material and construction along the length of pavement. High reliability yields high predicted cracking percentage along the length of pavement after a certain period in the design life of pavement, while a low-reliability yields low predicted cracking (NCHRP, 2003). Reported values of thicknesses in the results are the designed values obtained after rounding up the minimum required thickness to the nearest value that is a multiple of 5 mm.

### 2.5. Methodology for cost and GWP analysis

For the cost analysis of pavements (under the same loading conditions) for different mixes, firstly, the cost per unit cubic meter of

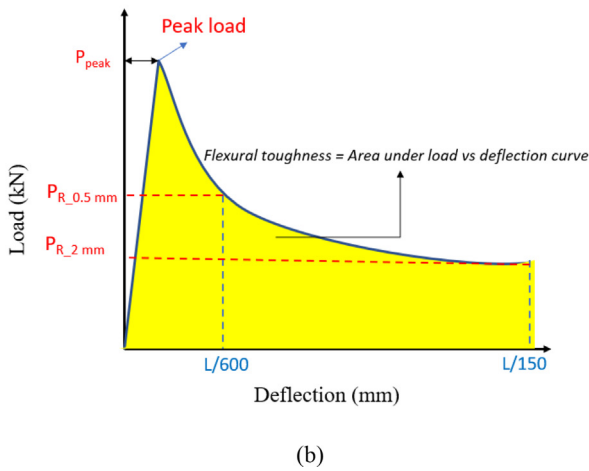
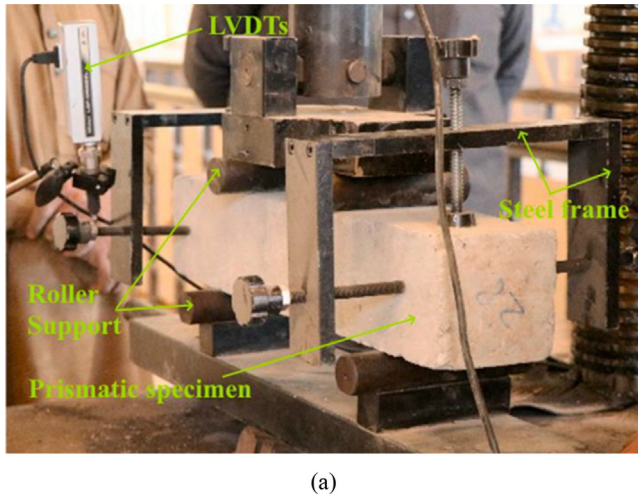


Fig. 2. Overview of (a) flexural testing setup (b) typical load versus mid-span deflection curve.

Table 4  
Traffic category/load spectrum and truck traffic.

Input parameter	Street 1	Street 2
Traffic category*	Collector	Major Arterial
Trucks traffic per day	500	1500
Growth rate	2%	2%
Design life of pavement	30-year	30-year
Direction distribution factor	50%	50%
Lane (designed) distribution factor	100%	100%
Average no. of truck traffic per day in design lane during whole design life	338	1,014
Total no. of trucks expected on design lane during the whole the design life	3,704,374	11,113,118

\* From PCA guidelines (Robert and Packard, 2007).

each concrete mix was calculated using the unit costs of raw materials, given in Table 6. In the absence of an up-to-date database, the unit costs of all ingredients of concrete batches were taken from a recent economic study published by Pakistani authors (Nawaz et al., 2020) considering similar materials. For all raw materials, the cost of transportation was included. Moreover, in the materials cost of concrete mixes, 20 USD per cubic meter was also added as the cost of transportation, mixing, placing, and labor. The cost of pavement per square meter for each mix was calculated using Eq. (1). To calculate the global warming potential (GWP) of each

Table 5  
Design parameters and properties of materials for both collector and major arterial streets.

General design parameters	
Serviceability at the end of design life	2 (fair)
Reliability-(R)	85%
Modulus of resilience ( $M_R$ ) of subgrade	28 MPa
The percentage of pavement cracked by the end of design life	15%
Composite-modulus of subgrade-reaction	28 MPa
Edge-support	Provided (at both sides)
Concrete material properties	
$f_R$ or Modulus of rupture (MPa)	Different for all mixes
$f_{RS}$ (%)	Different for FRCs* 0% for PC**
$E_C$ (MPa)	Different for all mixes
Macro-fibers	Considered for FRC No for PC

Table 6  
Unit costs of raw materials for concrete production (incl. transportation charges).

Material	Unit cost (USD/kg)
Portland cement (Nawaz et al., 2020)	0.1344
Quarry sand (Nawaz et al., 2020)	0.0065
Crushed limestone (Nawaz et al., 2020)	0.0109
Hooked steel fibers	0.8
Water (Nawaz et al., 2020)	0.0009
Superplasticizer (Nawaz et al., 2020)	1.45

mix, firstly carbon emissions ( $CO_2$ ) per cubic meter of each mix were calculated using the unit  $CO_2$  potential of raw materials, given in Table 7. Unit GWP potential of raw materials was taken from original research articles (Chan et al., 2019; Kurda et al., 2018) because no public data was available in Pakistan for the local materials. Therefore, the GWP potential of each material is taken from published research articles. Then this GWP per square meter of the pavement slab was calculated using Eq. (2).

$$CP = COST_{MIX} \times h_{Design} \quad (1)$$

where

$$CP = \text{Cost of pavement per square-meter (USD/m}^2\text{)}$$

$$COST_{MIX} = \text{Cost of each per cubic meter (USD/m}^3\text{)}$$

$$h_{Design} = \text{Design-thickness of pavement for a mix (m)}$$

$$GWP = CE_{MIX} \times h_{Design} \quad (2)$$

$$GWP = \text{Carbon emissions (kg-CO}_2\text{) per square meter of pavement (kg-CO}_2\text{/m}^2\text{)}$$

Table 7  
Carbon emissions per unit production of raw materials [cradle to grave].

Raw Material	Per unit energy emissions (kg-CO <sub>2</sub> /kg)
Portland cement (Kurda et al., 2018)	0.92
Fine aggregate (Kurda et al., 2018)	0.0015
Coarse aggregate (Kurda et al., 2018)	0.0285
Hooked steel fibers (Chan et al., 2019)	2.65
Water (Kurda et al., 2018)	0
SP (Kurda et al., 2018)	0.00181

$CE_{MIX}$  = Carbon emissions (kg-CO<sub>2</sub>) per cubic meter of concrete mix (CO<sub>2</sub>/m<sup>3</sup>)

$h_{Design}$  = Design thickness ( $h$ ) of pavement required for each concrete mix ( $m$ )

### 3. Results and discussion

#### 3.1. Compressive behavior

##### 3.1.1. Compressive strength ( $f_{CS}$ )

The  $f_{CS}$  test results of all mixes are presented in Fig. 3. It is apparent that the addition of fibers significantly increases the  $f_{CS}$  of concrete. The trend of increase in  $f_{CS}$  with the varying dosage of steel fiber is similar for all strength classes. The  $f_{CS}$  of low strength C20 improves by 3.3–9.1% with the addition of 0.25–1% steel fiber. Similarly, normal strength C30 and high strength C45 experience net gains of 3–11% and 6–13%, respectively, when the HSF percentage increases from 0.25 to 1%.

Advance in the  $f_{CS}$  of all strength classes because of fiber addition can be explained by several factors that lead to the strengthening of the binder matrix of the concrete. Firstly, the addition of fibers in the binder matrix improves the concrete's confinement that upgrades the compressive load-bearing capacity by controlling the lateral deformations (Ali et al., 2020a). Secondly, fibers prevent the cracking of microstructure due to dry shrinkage in the process of strength-gaining (Afroughsabet et al., 2017). Pre-existing microcracks in the binder matrix may proliferate at a faster rate under compressive loads in the case of plain concretes. Furthermore, HSF can restrict the propagation of cracks under loading and decrease the stress concentration at the ends (or tips) of cracks (Afroughsabet et al., 2017; Afroughsabet and Ozbakkaloglu, 2015).

HSF shows more net gain in the  $f_{CS}$  of high strength C45 than in the  $f_{CS}$  of low strength concrete. For example, at 1% HSF, C45 experiences a net gain of 13%, whereas the C20 at the same dosage experiences an increase of 9.1%. Similarly, C30 experiences a net gain of 11% which is also lower than observed in the case of C45. This development in the efficiency of fiber-reinforcement with  $f_{CS}$  increment can be ascribed to a stronger binder matrix in the case of C45 due to high cement content, whereas a less-strong or weak binder matrix is formed in the case of concretes (i.e., C20 and C30) with less cement content. Strengthening of the binder matrix/microstructure improves the efficiency of HSF-reinforcement in

resisting the tensile stresses (Ali et al., 2020b). Bond strength of HSF (due to interlocking between binder and hooks of HSF) also increases with the strengthening of microstructure. Good bond strength ensures efficient stress transmission between the binder matrix and fibers.

##### 3.1.2. Modulus of elasticity ( $E_C$ )

The  $E_C$  of each mix with varying HSF (%) is presented in Fig. 4. For all concrete classes, similar to  $f_{CS}$ ,  $E_C$  changes positively due to the inclusion of HSF. At 1% HSF,  $E_C$  of C20, C30, and C45 increases by 5.4%, 7.4%, and 9.7%, respectively.

Improvement in  $E_C$  due to HSF can be mainly explained by the increase in the axial and lateral stiffness of concrete that ultimately reduces the axial deformations in compression testing per unit stress. Simoes et al. (Simões et al., 2018) reported a slight increase in  $E_C$  at the 1.5% dosage of micro-steel fiber. Similar results were also reported by Thomas and Ramaswamy (2007). No reasons were given in these studies for the improvement in the  $E_C$  with steel fibers. Another study by Xie et al. (2018) reported a decrease of 10% in both  $f_{CS}$  and  $E_C$  due to the incorporation of thick steel fiber. They ascribed this behavior to the decrease in density of concrete with the inclusion of steel fiber. However, no such negative effects were noticed in the present study on both  $E_C$  and  $f_{CS}$ . The main difference between the study of Xie et al. and the present study is also that of the consideration to keep the workability. In this study, the plasticizer's dosage was increased to compensate for the loss in workability due to the inclusion of HSF, whereas, no such practice was adopted by Xie et al. rather they used a constant plasticizer dosage for both plain and steel fiber-reinforced concretes, which might have resulted in the production of less workable (or harsh) mixes in the case of fibrous mixes (Ali and Qureshi, 2019). Workability plays a significant role in achieving good compaction for mixes (Kurad et al., 2017). For the same compaction effort, a workable mix achieves more density than the harsh mix. Improvement in the density consequently leads to high strength. Reduction in the porosity or water accessible pore volume of concrete (possibly due to improvement in the density of mix) with the HSF inclusion of steel fiber in high-performance concrete (having good workability >120 mm) has been reported by Afroughsabet et al. (Afroughsabet et al., 2017). The reduction in the porosity can also attribute to the increase in the stiffness of concrete leading to an increase in  $E_C$ . Similar to results of  $f_{CS}$ , high strength C45 shows more positive behavior with HSF inclusion than low strength C20

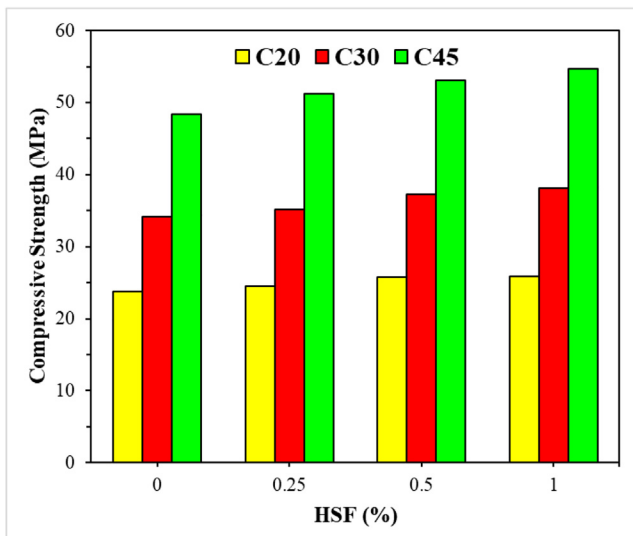


Fig. 3. Compressive testing results of each strength class with the HSF volume.

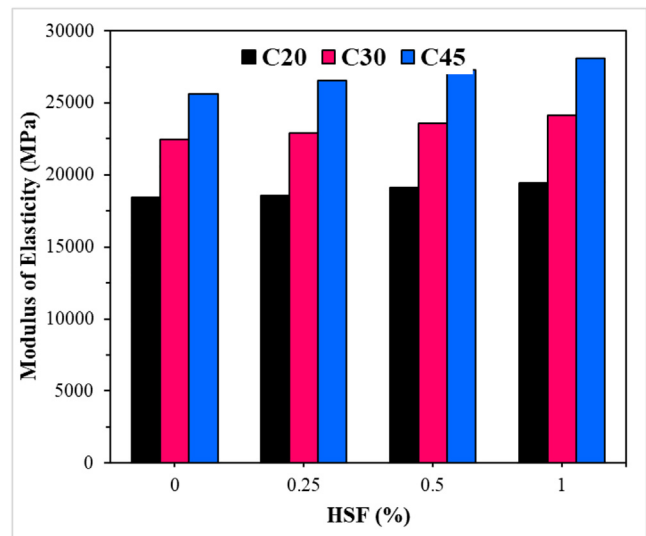


Fig. 4.  $E_C$  of each strength class with the varying HSF volume.

and C30. Highest net gains are noticed in the C45, and the lowest net gain is observed for C20. High strength binder matrix in case of C45 ensures stronger bond with binder matrix, unlike C20 and C30.

There is no substantial variance in the results of  $f_{CS}$  and  $E_c$  with the changing volume of HSF. The main reason for this behavior is the dependencies of both mechanical properties on the stiffness of concrete that improves with fiber addition. Earlier works also reported no substantial change between the behaviors of  $f_{CS}$  and  $E_c$  with the addition of fiber in the mix (Ayub et al., 2014; Daud et al., 2021; Thomas and Ramaswamy, 2007). Furthermore, an accurate relationship exists between the  $f_{CS}$  and  $E_c$  of concrete irrespective of the strength class and HSF volume, see Fig. 5. This relationship (see Eq. (3)) shows that without consideration of strength class and HSF volume of concrete,  $E_c$  can be estimated accurately from  $f_{CS}$ .

$$E_c = 3787\sqrt{f_{CS}} (20 \leq f_{CS} \leq 45\text{MPa}) \quad (3)$$

where  $E_c$  = modulus of elasticity (MPa) and  $f_{CS}$  = compressive strength (MPa)

### 3.2. Flexural behavior

#### 3.2.1. Flexural strength ( $f_R$ )

The flexural test results of all strength classes of concrete with varying doses of HSF are shown in Fig. 6. The results clearly show the importance of HSF in enhancing the flexural performance of the concrete. Due to fibers,  $f_R$  experiences expressively higher net gains compared to those in the case of  $f_{CS}$ . At 0.25–1% HSF, net gains in the  $f_R$  of C20, C30, and C45 are 20–49%, 25–57%, and 22–67%, respectively.

The main reason for the useful boost in  $f_R$  is the high efficiency of HSF in resisting tensile stresses. HSF increases the tensile stress-bearing capacity of concrete per unit tensile strain and prevents the propagation of micro and macro cracks (Afrouhsabet et al., 2017). Afrouhsabet et al. (2017) reported that the  $f_R$  of concrete improves by more than 80% with the addition of 1% double HSF. Carneiro et al. (2014) also reported a 39% increase in  $f_R$  with 0.75% HSF. The results of the present study are greatly in line with those of Carneiro et al. (2014). The high net gains in the  $f_R$  in the study of Afrouhsabet et al. (2017) could be because the use of double hook ended fibers provide excellent bond strength with binder matrix than that of the single hook end fibers used in the

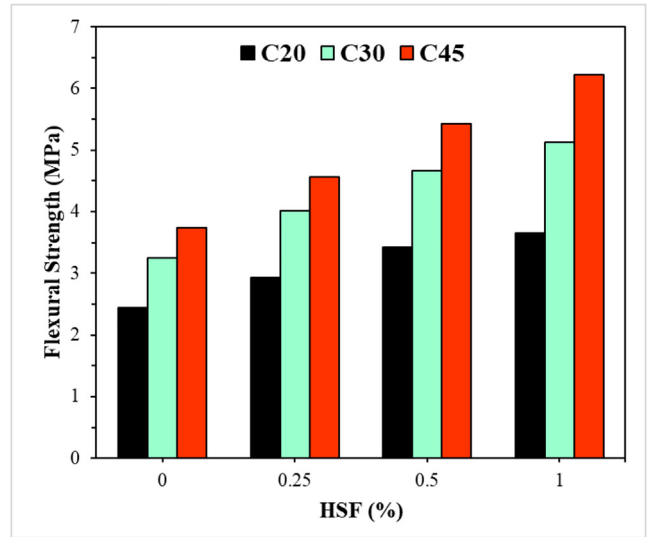


Fig. 6.  $f_R$  of each strength class with the varying HSF volume.

present study. But still, a phenomenal increase in the  $f_R$  was observed in the present study at the 1% HSF (49%, 57%, and 67%). Besides that, more strength increase with fiber addition was noticed in the case of C45 class of concrete. Earlier this has been ascribed to the stronger binder matrix in case of the high strength class compared to that of the low strength C20 and C30 classes. Previous studies (Al-Ghamdy et al., 1993; Chan and Chu, 2004; Wu et al., 2016) have also highlighted the importance of strengthening of binder matrix to increase the efficiency of steel fibers in mechanical properties. These studies showed that the pullout and bond strength of fiber improved with the development of the binder matrix. So, more pullout strength of fibers in the case of C45 led to higher net gains in its mechanical properties.

The relationship between  $f_{CS}$  and  $f_R$  of HSF-reinforced concretes cannot be accurately developed without considering the effect of the dosage of HSF. An accurate relationship can only be developed considering the role of reinforcement index in steel fiber-reinforced concretes (Thomas and Ramaswamy, 2007). In this study, these correlations were developed as shown in Fig. 7. These correlations (see Eqs. (4)–(6)) ( $R^2 > 0.85$ ) show good predictability of  $f_R$  from the  $f_{CS}$  of concrete, although, correlations should not be generalized because of a small number of sample points.

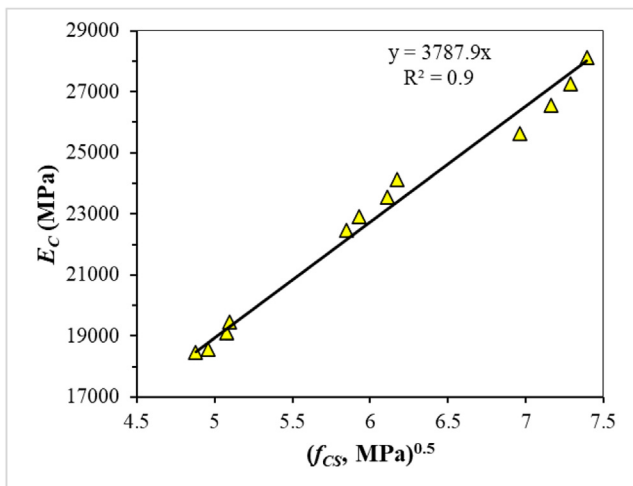


Fig. 5. Relationship between  $f_{CS}$  and  $E_c$  of concrete irrespective of strength class and HSF volume.

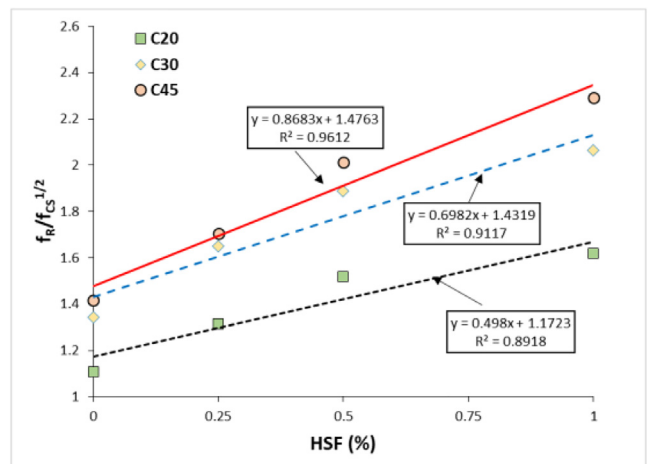


Fig. 7. Relationship between  $f_R/f_{CS}^{0.5}$  of each strength class and HSF (%).

$$f_R = (0.87V_F + 1.48)\sqrt{f_{CS}}(C20)$$

$$f_R = (0.70V_F + 1.43)\sqrt{f_{CS}}(C30)$$

$$f_R = (0.50V_F + 1.17)\sqrt{f_{CS}}(C45)$$

where  $f_R$  = flexural strength or modulus of rupture (MPa);  $f_{CS}$  = compressive strength of the particular strength class (MPa); and  $V_F$  = volume fraction of steel fiber (%)

3.2.2. Flexural toughness ( $T_R$ ) and residual strength ( $f_{RS}$ )

$T_R$  and  $f_{RS}$  were measured as stated by ASTM C1609 (2019). Load deflection results of flexural testing are given in Fig. 8. According to ASTM C1609,  $T_R$  of concrete is estimated by calculating under the whole length of the load–deflection curve up to the deflection of  $L/150$  (i.e.,  $L/150 = 300/150 = 2$  mm). Two-stage growth in these curves can be noticed in Fig. 8. These represent the ascending and descending developments in load–deflection curves before and after the peak stress. There is no substantial variance in the ascending curves of plain and fiber-reinforced concrete mixes. Although the increase in steel fiber dosage extends the length of ascending curves (indicating a noticeable increase in the peak load). Improvement in the length of the ascending curve is attributed to the increase in the flexural stiffness of concrete with the addition of steel fibers. Besides that, slopes of the descending curves become flat with the steel fiber. While plain mixes showed a very sharp negative slope after the peak load and attain a flat curve at very small loads. On the other hand, slopes of the descending curves for HSF mixes did not show a significant negative drop like plain mixes. Their slopes did not attain a flatter plateau, like plain mixes, at 0.5% and 1% HSF up to the deflection of  $L/150$  (2 mm). These developments indicate a substantial increase in the  $f_{RS}$  and  $T_R$  of all strength classes with HSF.

$T_R$  of each mix up to the deflection of  $L/150$  is shown in Fig. 9. These results show interesting developments such as the  $T_R$  of low strength C20 at 0.25% steel fiber was substantially higher than that of the plain high strength C45. No significant increase in  $T_R$  is noticed with the up-gradation of strength class of concrete.  $T_R$  of plain concrete increases by 7 and 18% by with the change in concrete class from low C20 to C45. Whereas these increments in the  $T_R$  are very small compared to those observed with the addition of HSF in low strength C20 (89%, 275% and 328% at 0.25%, 0.5%, and 1% HSF volume, respectively). These developments are attributed to the increase in the area under the descending curve with the addition of HSF. These results highlight the importance of fiber-reinforcement in enhancing the toughness of concrete and implies that the use of a small percentage of steel fiber is a better option than upgrading the strength class to acquire high  $T_R$ .  $f_{RS}$  is calculated using the load at  $L/150$  and  $L/600$  mm according to ASTM C1609 (2019) in the  $f_R$  (third-point loading) formula given in ASTM-C78 (2018a) and ASTM-C78 (2018b). It is an important input parameter for the thickness design of pavement when pavements are designed for mixes incorporating macro-fibers (Robert and Packard, 2007).  $f_{RS}$  as the percentage of peak strength or  $f_R$  at the peak load of each mix is shown in Fig. 10. The results of  $f_{RS}$  show that it is that each strength class retains a similar percentage of residual strength at  $L/150$  deflection. Each class of concrete retained  $f_{RS}$  of 16–18%, 24–28%, 34–37% at 0.25%, 0.5% and 1% HSF.

3.3. Design thickness of pavement ( $h_{Design}$ )

Using the mechanical properties of concrete i.e.  $f_R$ ,  $f_{RS}$ , and  $E_C$  and other design inputs given in Tables 4 and 5,  $h_{Design}$  for the collector and major arterial pavements was calculated based on the

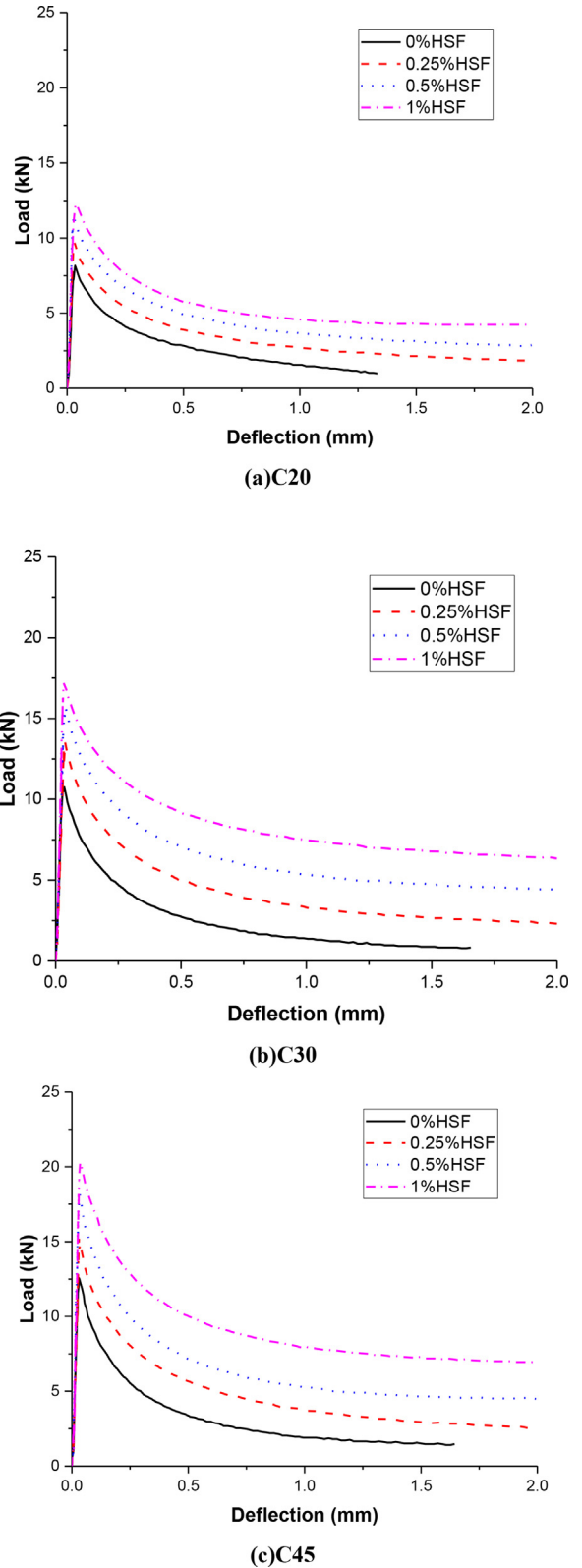


Fig. 8. Load-deflection behavior of (a) C20 strength class (b) C30 strength class and (c) C45 strength class with the variation in HSF volume.

PCA mechanistic design of pavements (Robert and Packard, 2007). The analysis shows that  $h_{Design}$  reduces for both collector and major arterial significantly with the addition of HSF, see Fig. 11.  $h_{Design}$  of both collector and major arterial street pavements

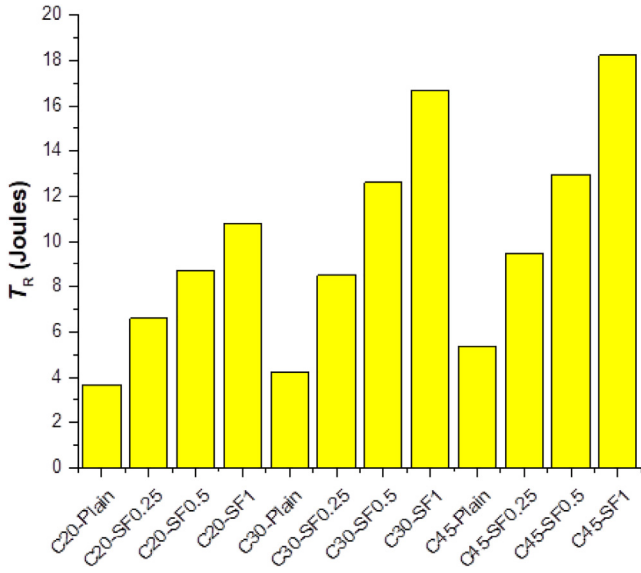


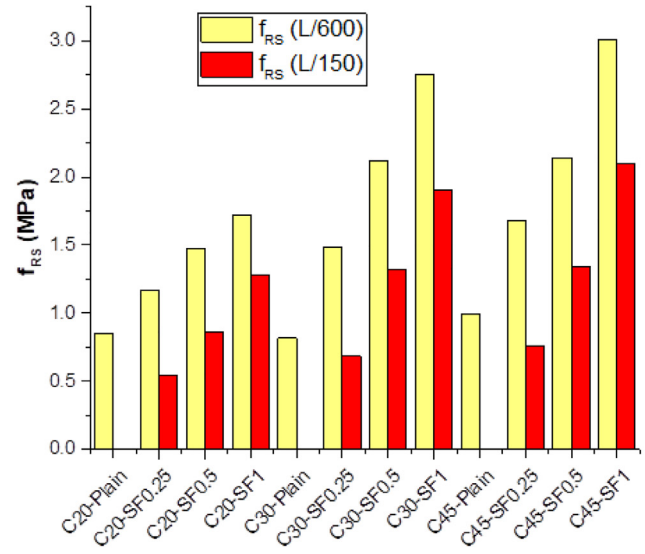
Fig. 9. Flexural toughness ( $T_R$ ) of C20, C30 and C45 concrete classes with the varying HSF volume.

reduces by 40%, 32%, and 27% for C20, C30, and C45 concrete with the addition of HSF (depending upon the dosage). In the case of collector pavements (where truck traffic is light) no significant reduction is noticed in  $h_{Design}$  beyond 0.25% steel fiber for the C30 and C45 class of concrete. Whereas, in the case of low strength C20 no significant decrease in  $h_{Design}$  is noticed beyond 0.5% HSF. The minimum possible  $h_{Design}$  of 135 mm is almost met at a 0.50% HSF in all strength classes for collector pavement. These results imply no usefulness of 1%HSF in the reduction of  $h_{Design}$ .

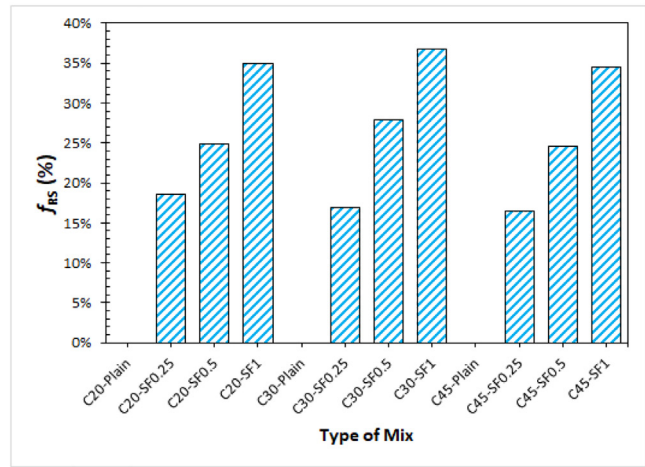
On the other hand, in the case of major arterial JPCP (where truck traffic is high compared to collector pavement), the minimum possible thickness of 170 mm is almost achieved at 0.5% HSF for C30 and C45. No significant difference is noticed in the  $h_{Design}$  of both collectors and arterial pavements at 0.5% and 1% HSF irrespective of strength class of concrete. These results show the usefulness of incorporating HSF in any mix to decrease the  $h_{Design}$  without increasing the  $f_{CS}$  class of concrete (increasing the cement content). Even though increasing the strength class of concrete reduces the  $h_{Design}$ , the difference in the thickness values of pavement between strength classes reduces with the increasing the dosage of fiber. This means at 1% steel fiber; all strength classes of concrete provide almost the same  $h_{Design}$ .

3.4. Cost and global warming potential (GWP) of pavements

Detailed cost analysis of the mixes shows that after superplasticizer (SP), HSF is the most expensive material per unit quantity (USD/kg). An increase in the HSF dose from 0 to 1%, raises the cost of a concrete mix by more than 70%. Besides that, an increase in the demand for plasticizers due to the addition of macro-fibers also increases the final cost of product fibrous concrete. But the analysis of the cost per square meter of pavements for all mixes tells a different story for the same service conditions, (truckloads, traffic category, service life, etc.) see Table 8. The cost of pavement for all strength classes is minimum at 0.25 and 0.5% HSF (significantly lower than that of the plain concretes). Moreover, both plain and highly reinforced mixes show a higher cost of pavement values for a particular strength class than the mixes with intermediate dosages of fiber i.e., 0.25–0.5% HSF. These trends are similar for both collectors and major arterial pavements. A significant reduction in pavement thickness due to the increase in the  $f_R$  of concrete



(a)



(b)

Fig. 10. (a)  $f_{RS}$  of C20, C30 and C45 classes of concrete with the varying HSF volume at the deflections of L/600 and L/150 i.e. 0.5 mm and 2 mm (b)  $f_{RS}$  as the percentage of peak strength or  $f_R$ .

with HSF addition reduces the cost per square meter of pavement. Since no noticeable reduction in the pavement thickness is noticed

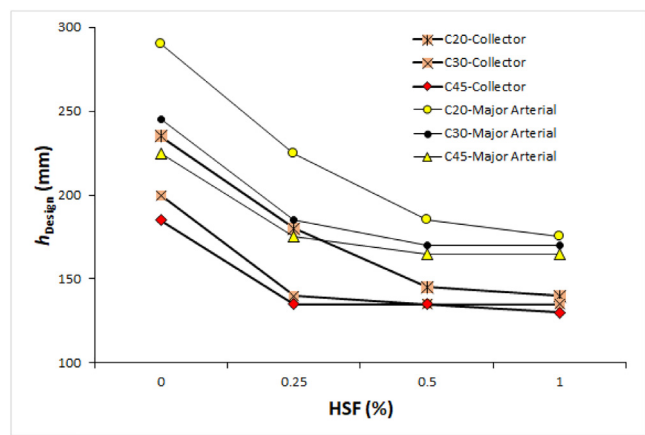


Fig. 11. Influence of HSF on the  $h_{Design}$  of pavements for C20, C30, and C45.

**Table 8**  
Cost per m<sup>2</sup> of pavement (CP) for all mixes.

Mix ID	Cement (USD)	Water (USD)	Aggregates (USD)		HSF (USD)	SP (USD)	Total Cost* (USD/m <sup>3</sup> )	Design thickness (m)		Cost per m <sup>2</sup> CP** (USD/m <sup>2</sup> )	
			Coarse Aggregate	Fine aggregate				Collector	Major Arterial	Collector	Major Arterial
C20-HSF0	34.3	0.162	12	6	0	0.0	71.77	0.235	0.29	16.9	20.8
C20-HSF0.25	34.3	0.162	12	6	15.6	0.9	88.20	0.18	0.225	15.9	19.8
C20-HSF0.5	34.3	0.162	12	6	31.2	1.3	104.16	0.145	0.185	15.1	19.3
C20-HSF1	34.3	0.162	12	6	62.4	2.4	136.31	0.14	0.175	19.1	23.9
C30-HSF0	44.4	0.162	12	6	0	0.0	81.85	0.2	0.245	16.4	20.1
C30-HSF0.25	44.4	0.162	12	6	15.6	1.1	98.55	0.14	0.185	<b>13.8</b>	<b>18.2</b>
C30-HSF0.5	44.4	0.162	12	6	31.2	1.7	114.62	0.135	0.17	15.5	19.5
C30-HSF1	44.4	0.162	12	6	62.4	3.1	147.09	0.135	0.17	<b>19.9</b>	<b>25.0</b>
C45-HSF0	63.8	0.162	12	6	0	0.0	101.34	0.185	0.225	18.7	22.8
C45-HSF0.25	63.8	0.162	12	6	15.6	1.7	118.54	0.135	0.175	16.0	20.7
C45-HSF0.5	63.8	0.162	12	6	31.2	2.4	134.84	0.135	0.165	18.2	22.2
C45-HSF1	63.8	0.162	12	6	62.4	4.4	167.92	0.13	0.165	21.8	27.7

\*Total cost: including 20\$ for mixing, transportation and casting;

\*\*CP is obtained by using Eq.(1).

**Table 9**  
GWP per m<sup>2</sup> of pavement for all mixes.

Mix IDS	Cement (kg-CO <sub>2</sub> )	Aggregates (kg-CO <sub>2</sub> )		Steel fiber (kg-CO <sub>2</sub> )	SP (kg-CO <sub>2</sub> )	Total (CO <sub>2</sub> /m <sup>3</sup> )	Design thickness (m)		GWP per m <sup>2</sup>	
		Coarse aggregate	Fine aggregate				Collector	Major Arterial	Collector	Major Arterial
C20-HSF0	235	31	1.30	0	0.0000	267	0.24	0.29	63	77
C20-HSF0.25	235	31	1.29	52	0.0011	318	0.18	0.23	<b>57</b>	<b>72</b>
C20-HSF0.5	235	30	1.29	103	0.0016	370	0.15	0.19	<b>54</b>	<b>68</b>
C20-HSF1	235	30	1.28	207	0.0030	473	0.14	0.18	66	83
C30-HSF0	304	31	1.30	0	0.0000	336	0.20	0.25	67	82
C30-HSF0.25	304	31	1.29	52	0.0014	387	0.14	0.19	<b>54</b>	<b>72</b>
C30-HSF0.5	304	30	1.29	103	0.0021	439	0.14	0.17	<b>59</b>	<b>75</b>
C30-HSF1	304	30	1.28	207	0.0038	542	0.14	0.17	73	92
C45-HSF0	437	31	1.30	0	0.0000	469	0.19	0.23	87	106
C45-HSF0.25	437	31	1.29	52	0.0021	521	0.14	0.18	70	91
C45-HSF0.5	437	30	1.29	103	0.0030	572	0.14	0.17	77	94
C45-HSF1	437	30	1.28	207	0.0055	675	0.13	0.17	88	111

beyond 0.5% HSF in cases of both collector and arterial streets, therefore, cost of pavement values of mixes with 1%HSF drastically increase due to very high per-unit cost of the mix. Using low strength concrete C20 with 0.25–0.5%HSF, the cost of pavement values better than that of the plain C30 and C45 concretes can be achieved. The minimum cost for the same design loadings is related to C30-HSF0.25%. After that, C20-HSF0.25% and C20-HSF0.5% and C30-HSF0.5% show minimum cost values.

GWP analysis of the pavement designed for all mixes is presented in Table 9. Even if HSF is the material with the highest carbon footprint per unit quantity (CO<sub>2</sub>), the results of GWP per square meter of pavement suggest the usefulness of HSF in controlling the carbon emissions by reducing the consumption of raw materials for concrete manufacturing. Analysis of these results also suggests that choosing the high strength concrete i.e., C45 for pavements is less eco-friendly than choosing low strength C20 and normal strength C30 concretes with HSF for the same performance in the applications of collector and major arterial pavements. Increasing the cement quantity for the sake of upgrading the  $f_r$  significantly increases the GWP per square meter of pavement, instead, using low cement concretes like C20 and C45 concretes with 0.25–0.5% HSF, high  $f_r$  can be acquired and besides that, the GWP of pavement is also reduced (compare to that of the plain concrete). Unlike the results of cost analysis, no significant difference is noticed between the GWP values for the plain and highly reinforced mixes. For example, in the case of high strength C45, there is no noticeable difference in the GWP values of plain (HSC-Plain) and highly reinforced mix (HSC-1%SF). This is because of a significant reduction in CO<sub>2</sub> caused by the decreased  $h_{Design}$  of the pavement.

Results of both cost and GWP analysis show that the economic and environmental performance of fiber-reinforced mixes should not be judged by their per-unit production cost or GWP (i.e., USD/m<sup>3</sup> and CO<sub>2</sub>/m<sup>3</sup>), instead, their application should be considered in mind while evaluating their economic and environmental performances. Despite a very high carbon footprint and material costs per unit production for fibrous mixes, the requirements of quantities of these mixes for the same application are very small compared to those of the plain concretes. Fiber-reinforced mixes are eco-friendly and cheap for the same service requirements that plain concrete would provide. Not only fiber-reinforced mixes (with 0.25–0.5%SF) provide economy and eco-friendliness, but their applications may also reduce the quantities of natural resources that can be saved for future developments. For example, reduction 40% thickness with 0.5% SF, ensures savings of cement, coarse and fine aggregates, etc. These results imply all three benefits with fibrous reinforced concrete applications over plain concretes i.e., economy, eco-friendliness, and sustainability. Based on these benefits combined, C20-HSF0.5%, C30-HSF0.25%, and C30-HSF0.5% can be taken as optimum mixes.

#### 4. Conclusions

Concretes of all strength classes experienced a rise in mechanical properties with the increasing HSF dosage. Compressive strength and modulus of elasticity of all strength classes (C20, C30, and C45) were moderately improved due to HSF addition. Mechanical properties of high strength C45 were more positively

affected compared to low strength classes (i.e., C20 and C30) due to fiber incorporation. A significant effect of fiber addition was observed on the flexural behavior of all strength classes. Owing to improvement in the bond performance, the efficiency of HSF increased with the rise in strength class of concrete. The role of fibers was very phenomenal in the flexural behavior, such that, low strength C20 yielded better toughness and residual strength than plain high strength C45. This showed that using fibers is an effective method in upgrading the overall flexural behavior of plain concrete compared to using a high quantity of cement. C20 and C30 concretes with 0.25%HSF, yielded higher flexural toughness than that of the plain high strength C45.

The maximum reductions in the design thickness of pavement were observed at 0.25 and 0.5% addition of HSF in all strength classes. Low strength C20 with 0.25–1% HSF yielded smaller design thickness than plain high strength C45 under the same loading conditions. Low strength concretes (i.e., C20 and C30) with a small HSF volume can yield better economic performance than plain high strength concretes for the same service.

Despite having a high carbon footprint per unit volume, HSF-reinforced concrete with 0.25–0.5% HSF volume showed lower global warming potential (GWP) compared to plain concretes for the loading conditions. The mixes showing minimum GWP belong to the C20 and C30 concretes with intermediate HSF volumes (i.e., 0.25% and 0.5%). Both highly reinforced mixes (with 1%HSF) and plain mixes are uneconomical and environmentally harmful.

## 5. Availability of data and material

All data and materials used are provided in this research article.

## 6. Code availability

Not applicable.

## Funding

No external funding was received during the life cycle of this project.

## Declaration of Competing Interest

The authors declare that they have no known competing financial interests or personal relationships that could have appeared to influence the work reported in this paper.

## References

AASHTO, 2009. AASHTO. Guide for Design of Pavement Structures. ACI-211.1-91, 2000. Standard practice for selecting proportions for normal, heavyweight, and mass concrete. ACI Manual of Concrete Practice 2000, Part 1: Materials and General Properties of Concrete. American Concrete Institute.

Afroughsabet, V., Biolzi, L., Monteiro, P.J.M., 2018. The effect of steel and polypropylene fibers on the chloride diffusivity and drying shrinkage of high-strength concrete. *Compos. B Eng.* 139, 84–96.

Afroughsabet, V., Biolzi, L., Ozbakkaloglu, T., 2017. Influence of double hooked-end steel fibers and slag on mechanical and durability properties of high performance recycled aggregate concrete. *Compos. Struct.* 181, 273–284.

Afroughsabet, V., Ozbakkaloglu, T., 2015. Mechanical and durability properties of high-strength concrete containing steel and polypropylene fibers. *Constr. Build. Mater.* 94, 73–82. <https://doi.org/10.1016/j.conbuildmat.2015.06.051>.

Afroz, M., Venkatesan, S., Patnaikuni, I., 2019. Effects of hybrid fibers on the development of high volume fly ash cement composite. *Constr. Build. Mater.* 215, 984–997. <https://doi.org/10.1016/j.conbuildmat.2019.04.083>.

Ahmadi, M., Farzin, S., Hassani, A., Motamedi, M., 2017. Mechanical properties of the concrete containing recycled fibers and aggregates. *Constr. Build. Mater.* 144, 392–398.

Al-Ghamdy, D.O., Tons, E., Wight, J.K., 1993. Effect of matrix composition on steel fiber reinforced concrete properties. *J. King Saud Univ. – Eng. Sci.* 5 (1), 55–75. [https://doi.org/10.1016/S1018-3639\(18\)30571-3](https://doi.org/10.1016/S1018-3639(18)30571-3).

Al Qadi, A.N.S., Al-Zaidyeen, S.M., 2014. Effect of fibre content and specimen shape on residual strength of polypropylene fibre self-compacting concrete exposed to elevated temperatures. *J. King Saud Univ. – Eng. Sci.* 26 (1), 33–39. <https://doi.org/10.1016/j.jksues.2012.12.002>.

Algburi, A.H.M., Sheikh, M.N., Hadi, M.N.S., 2019. Mechanical properties of steel, glass, and hybrid fiber reinforced reactive powder concrete. *Front. Struct. Civil Eng.* 13 (4), 998–1006.

Ali, B., Qureshi, L.A., 2019. Influence of glass fibers on mechanical and durability performance of concrete with recycled aggregates. *Constr. Build. Mater.* 228, 116783. <https://doi.org/10.1016/j.conbuildmat.2019.116783>.

Ali, B., Qureshi, L.A., Shah, S.H.A., Rehman, S.U., Hussain, I., Iqbal, M., 2020a. A step towards durable, ductile and sustainable concrete: Simultaneous incorporation of recycled aggregates, glass fiber and fly ash. *Constr. Build. Mater.* 251, 118980. <https://doi.org/10.1016/j.conbuildmat.2020.118980>.

Ali, B., Raza, S.S., Hussain, I., Iqbal, M., 2020b. Influence of different fibers on mechanical and durability performance of concrete with silica fume in press Struct. *Concr.* 22 (1), 318–333. <https://doi.org/10.1002/suco.v22.110.1002/suco.201900422>.

ASTM-C150, 2018. In: ASTM C150 Standard Specification for Portland Cement. ASTM International, West Conshohocken, PA, USA. [https://doi.org/10.1520/C0150\\_C0150M-18](https://doi.org/10.1520/C0150_C0150M-18).

ASTM-C1609, 2019. Standard Test Method for Flexural Performance of Fiber-Reinforced Concrete (Using Beam With Third-Point Loading). ASTM International, West Conshohocken, PA.

ASTM-C33, 2018. Standard Specification for Concrete Aggregates. ASTM International, West Conshohocken, PA, USA.

ASTM-C469, 2014. Standard Test Method for Static Modulus of Elasticity and Poisson's Ratio of Concrete in Compression. ASTM International, West Conshohocken, PA, USA.

ASTM-C78, 2018a. Standard Test Method for Flexural Strength of Concrete (Using Simple Beam with Third-Point Loading). ASTM Standards. ASTM International, West Conshohocken, PA, USA.

ASTM-C78, 2018b. Standard test method for flexural strength of concrete (using simple beam with third-point loading). ASTM Standards. ASTM International, West Conshohocken, PA, USA.

ASTM, C., 2012. Standard test method for compressive strength of cylindrical concrete specimens. ASTM C39/C39M-12.

Ayub, T., Shafiq, N., Nuruddin, M.F., 2014. Mechanical properties of high-performance concrete reinforced with basalt fibers. *Procedia Eng.* 77, 131–139.

Balendran, R.V., Zhou, F.P., Nadeem, A., Leung, A.Y.T., 2002. Influence of steel fibres on strength and ductility of normal and lightweight high strength concrete. *Build. Environ.* 37 (12), 1361–1367.

Bentur, A., Mindess, S., 2007. Fibre reinforced cementitious composites. *Modern Concrete Technology*, . .

Carneiro, J.A., Lima, P.R.L., Leite, Mônica.B., Toledo Filho, R.D., 2014. Compressive stress-strain behavior of steel fiber reinforced-recycled aggregate concrete. *Cem. Concr. Compos.* 46, 65–72.

Chan, R., Santana, M.A., Oda, A.M., Paniguel, R.C., Vieira, L.B., Figueiredo, A.D., Galobardes, I., 2019. Analysis of potential use of fibre reinforced recycled aggregate concrete for sustainable pavements. *J. Cleaner Prod.* 218, 183–191. <https://doi.org/10.1016/j.jclepro.2019.01.221>.

Chan, Y.-W., Chu, S.-H., 2004. Effect of silica fume on steel fiber bond characteristics in reactive powder concrete. *Cem. Concr. Res.* 34 (7), 1167–1172. <https://doi.org/10.1016/j.cemconres.2003.12.023>.

Daud, R.A., Daud, S.A., Al-Azzawi, A.A., 2021. Tension stiffening evaluation of steel fibre concrete beams with smooth and deformed reinforcement. *J. King Saud Univ. – Eng. Sci.* 33 (3), 147–152. <https://doi.org/10.1016/j.jksues.2020.03.002>.

Fareed, S., Behinaein, P., Almonbhi, A., Sindi, W., Alluqmani, A., 2021. Bridge steel fiber reinforced concrete specimens under high loading rates. *J. King Saud Univ. – Eng. Sci.* <https://doi.org/10.1016/j.jksues.2021.08.011>.

Han, J., Zhao, M., Chen, J., Lan, X., 2019. Effects of steel fiber length and coarse aggregate maximum size on mechanical properties of steel fiber reinforced concrete. *Constr. Build. Mater.* 209, 577–591. <https://doi.org/10.1016/j.conbuildmat.2019.03.086>.

Karahan, O., Atiş, C.D., 2011. The durability properties of polypropylene fiber reinforced fly ash concrete. *Mater. Des.* 32 (2), 1044–1049.

Kurad, R., Silvestre, José.D., de Brito, J., Ahmed, H., 2017. Effect of incorporation of high volume of recycled concrete aggregates and fly ash on the strength and global warming potential of concrete. *J. Cleaner Prod.* 166, 485–502.

Kurda, R., Silvestre, J.D., de Brito, J., 2018. Life cycle assessment of concrete made with high volume of recycled concrete aggregates and fly ash. *Resour. Conserv. Recycl.* 139, 407–417.

Nawaz, M.A., Qureshi, L.A., Ali, B., Raza, A., 2020. Mechanical, durability and economic performance of concrete incorporating fly ash and recycled aggregates. *SN Appl. Sci.* 2, 162. <https://doi.org/10.1007/s42452-020-1960-8>.

NCHRP, 2003. Guide for Mechanistic-Empirical Design of new and rehabilitated pavement structures.

Raza, S.S., Qureshi, L.A., Ali, B., Raza, A., Khan, M.M., 2020a. Effect of different fibers (steel fibers, glass fibers and carbon fibers) on mechanical properties of reactive powder concrete (RPC) in press Struct. *Concr.* 22 (1), 334–346. <https://doi.org/10.1002/suco.v22.110.1002/suco.201900439>.

Raza, S.S., Qureshi, L.A., Ali, B., Raza, A., Khan, M.M., Salahuddin, H., 2020b. Mechanical properties of hybrid steel-glass fiber-reinforced reactive powder concrete after exposure to elevated temperatures. *Arab. J. Sci. Eng.* 45 (5), 4285–4300. <https://doi.org/10.1007/s13369-020-04435-4>.

- Robert, G., Packard, P.E., 2007. Thickness Design for Concrete Highway and Street Pavements: Portland Cement Association (Using ACPA Thickness Design Tool Street Pave).
- Simões, T., Costa, H., Dias-da-Costa, D., Júlio, E., 2018. Influence of type and dosage of micro-fibres on the physical properties of fibre reinforced mortar matrixes. *Constr. Build. Mater.* 187, 1277–1285.
- Thomas, J., Ramaswamy, A., 2007. Mechanical properties of steel fiber-reinforced concrete. *J. Mater. Civ. Eng.* 19 (5), 385–392.
- Wu, Z., Shi, C., Khayat, K.H., 2016. Influence of silica fume content on microstructure development and bond to steel fiber in ultra-high strength cement-based materials (UHSC). *Cem. Concr. Compos.* 71, 97–109. <https://doi.org/10.1016/j.cemconcomp.2016.05.005>.
- Xie, J., Zhang, Z., Lu, Z., Sun, M., 2018. Coupling effects of silica fume and steel-fiber on the compressive behaviour of recycled aggregate concrete after exposure to elevated temperature. *Constr. Build. Mater.* 184, 752–764. <https://doi.org/10.1016/j.conbuildmat.2018.07.035>.
- Zain, M.F.M., Mahmud, H.B., Ilham, A., Faizal, M., 2002. Prediction of splitting tensile strength of high-performance concrete. *Cem. Concr. Res.* 32 (8), 1251–1258.
- Zhang, P., Li, Q.-fu., 2013. Effect of polypropylene fiber on durability of concrete composite containing fly ash and silica fume. *Compos. B Eng.* 45 (1), 1587–1594.